



# 1 The catastrophic thermokarst lake drainage events of 2018 in 2 northwestern Alaska: Fast-forward into the future

3 Ingmar Nitze<sup>1</sup>, Sarah Cooley<sup>2</sup>, Claude Duguay<sup>3,4</sup>, Benjamin M. Jones<sup>5</sup>, Guido Grosse<sup>1,6</sup>

4 <sup>1</sup>Alfred Wegener Institute for Polar and Marine Research, Potsdam, 14473 Potsdam, Germany

5 <sup>2</sup>Department of Earth, Environmental and Planetary Sciences, Brown University, Providence, RI, 02912, USA

6 <sup>3</sup>Department of Geography and Environmental Management, University of Waterloo, Waterloo, Canada

7 <sup>4</sup>H2O Geomatics Inc., Waterloo, Canada

8 <sup>5</sup>Institute of Northern Engineering, University of Alaska Fairbanks, Fairbanks, Alaska, 99775, USA

9 <sup>6</sup>University of Potsdam, Institute of Geosciences, 14476 Potsdam, Germany

10 *Correspondence to:* Ingmar Nitze (ingmar.nitze@awi.de)

## 11 **Abstract.**

12 Northwestern Alaska has been highly affected by changing climatic patterns with new temperature and precipitation maxima  
13 over the recent years. In particular, the Baldwin and northern Seward peninsulas are characterized by an abundance of  
14 thermokarst lakes that are highly dynamic and prone to lake drainage, like many other regions at the southern margins of  
15 continuous permafrost. We used Sentinel-1 synthetic aperture radar (SAR) and Planet CubeSat optical remote sensing data to  
16 analyze recently observed widespread lake drainage. We then used synoptic weather data, climate model outputs and lake-ice  
17 growth simulations to analyze potential drivers and future pathways of lake drainage in this region. Following the warmest  
18 and wettest winter on record in 2017/2018, 192 lakes were identified to have completely or partially drained in early summer  
19 2018, which exceeded the average drainage rate by a factor of ~10 and doubled the rates of the previous extreme lake drainage  
20 years of 2005 and 2006. The combination of abundant rain- and snowfall and extremely warm mean annual air temperatures  
21 (MAAT), close to 0° C, may have led to the destabilization of permafrost around the lake margins. Rapid snow melt and high  
22 amounts of excess meltwater further promoted rapid lateral breaching at lake shores and consequently sudden drainage of  
23 some of the largest lakes of the study region that likely persisted for millenia. We hypothesize that permafrost destabilization  
24 and lake drainage will accelerate and become the dominant drivers of landscape change in this region. Recent MAAT are  
25 already within the range of predictions by UAF SNAP ensemble climate predictions in scenario RCP6.0 for 2100. With MAAT  
26 in 2019 exceeding 0° C at the nearby Kotzebue, Alaska climate station for the first time since continuous recording started in  
27 1949, permafrost aggradation in drained lake basins will become less likely after drainage, strongly decreasing the potential  
28 for freeze-locking carbon sequestered in lake sediments, signifying a prominent regime shift in ice-rich permafrost lowland  
29 regions.

30



31 Keywords: Permafrost, permafrost thaw, thermokarst, lake change, lake drainage, Seward Peninsula, Baldwin Peninsula,  
32 Alaska

### 33 **1 Introduction**

34 Permafrost is widespread (20 to 25 % of the land area) in the northern high latitudes (Brown et al., 1997; Obu et al., 2019) and  
35 is primarily a result of past and present cold climatic conditions (Shur and Jorgenson, 2007). The rapidly warming Arctic  
36 climate is already reducing the stability and distribution of near-surface permafrost. Warming of permafrost at the global scale  
37 has been observed over recent decades from borehole temperature measurements (Romanovsky et al., 2010; Biskaborn et al.,  
38 2019), while local to regional permafrost degradation has been observed in many studies of varying scales across the permafrost  
39 domain (Nitze et al. 2018). Widespread near-surface permafrost loss or transition from continuous to discontinuous permafrost  
40 has for example been shown with remote sensing-supported permafrost modeling in Alaska (Pastick et al., 2015). Permafrost  
41 degradation may lead to long-term surface subsidence (Streletskiy et al., 2017), change in hydrological regimes (Liljedahl et  
42 al., 2015), and release of greenhouse gases carbon dioxide (CO<sub>2</sub>), methane (CH<sub>4</sub>), or nitrous oxide (N<sub>2</sub>O) (Elberling et al.,  
43 2013; Walter Anthony et al., 2018; Repo et al., 2009). In particular, the release of greenhouse gases from carbon locked away  
44 for thousands of years will trigger further warming through the permafrost carbon feedback (Schuur et al., 2015). Furthermore,  
45 the stability of permafrost is crucial for local communities which are dependent on ground stability for infrastructure, food  
46 security, and water supply (Chambers et al., 2007; White et al., 2007; Melvin et al., 2017; Hjord et al., 2018).

47 Rapid changes in lake area, including expansion and drainage, are strong indicators of permafrost degradation and thaw (Smith  
48 et al., 2005; Hinkel et al., 2007; Jones et al., 2011; Grosse et al., 2013; Arp et al., 2018; Nitze et al., 2018a). Natural lake  
49 drainage has been associated with near-surface permafrost degradation such as melting of ice wedges, formation of thermo-  
50 erosional channels, gully headward erosion, or internal drainage through permafrost-penetrating taliks (Mackay, 1988;  
51 Yoshikawa and Hinzman, 2003; Hinkel et al., 2007; Marsh et al., 2009; Jones et al., 2020a). Other natural lake drainage events  
52 have been connected to increased precipitation, causing bank overtopping with subsequent drainage channel formation, or  
53 snow dams and subsequent outburst floods and drainage channel formation (Mackay, 1988; Jones and Arp, 2015).

54 The southern margin of continuous permafrost in northwestern, western and interior Alaska as well as adjacent northwestern  
55 Canada has been identified as a region with a high temporal variability in lake area, and particularly widespread lake drainage  
56 (Jones et al., 2011; Chen et al., 2014; Lantz and Turner, 2015; Nitze et al., 2018a). Over the past few decades, lake drainage  
57 has outpaced lake growth by 14.9 % on the Seward Peninsula in western Alaska, largely driven by the drainage of several very  
58 large individual lakes (Jones et al., 2011; Nitze et al., 2017). Other transitional permafrost regions around the Arctic are broadly  
59 affected by the same pattern, with widespread drainage events and total area of lake loss exceeding total area of lake expansion  
60 (Smith et al., 2005; Nitze et al., 2018a). However, lakes also experience intra-annual (Cooley et al., 2017, 2019) to multi-year  
61 (Plug et al., 2008; Karlsson et al., 2014) water level fluctuations linked to precipitation and evaporation dynamics or overall  
62 hydrological runoff regimes, which can cause high uncertainty in interpreting temporally sparse observations. In particular,



63 recently shifting weather patterns with warmer air and sea surface temperatures along Arctic coasts driven by reduced sea ice  
64 cover (Bhatt et al., 2014) may also have an effect on coastal lowland permafrost (Lawrence and Slater, 2005) and thus  
65 potentially lake dynamics (Alexeev et al., 2016; Arp et al., 2019). For example, persistent warm air and sea surface  
66 temperatures caused a new sea ice minimum in the Bering Sea west of Alaska resulting in unprecedented largely open seas in  
67 the winter 2017/2018 (Stabeno and Bell, 2019) .

68 Other regions with cold continuous permafrost (e.g., Arctic Coastal Plain, Tuktoyaktuk Peninsula, Coastal Lowlands of  
69 Siberia) are also affected by lake drainage (Hinkel et al., 2007; Kravtsova and Bystrova, 2009; Karlsson et al., 2012; Lantz  
70 and Turner, 2015; Olthof et al., 2015; Nitze et al., 2017, 2018; Jones et al., 2020a), but to a lesser intensity than the transitional  
71 zone towards discontinuous permafrost, particularly in Alaska and western Siberia (Nitze et al., 2017, 2018).

72 Several studies suggest that lake drainage might be episodic with drainage events clustered in time and therefore potentially  
73 related to specific environmental conditions, such as high precipitation events (Marsh et al., 2009; Swanson, 2019; Jones et  
74 al., 2020a). Others, in contrast, find more stable to decreasing, long-term drainage rates, e.g. in northern Alaska and the Western  
75 Canadian Arctic (Hinkel et al., 2007; Marsh et al., 2009; Jones et al., 2020a).

76 In western Alaska, a series of major drainage events took place in the mid-2000s, where some of the largest thermokarst lakes  
77 on the ground-ice rich northern Seward Peninsula drained within a short period of a few years (Jones et al., 2011; Swanson,  
78 2019). The recent drainage of several large lakes on the northern Seward Peninsula and the largest lake on the Baldwin  
79 Peninsula provides an interesting test bed for analyzing lake drainage progression in high temporal and spatial detail using  
80 remote sensing imagery, meteorological data, and lake ice characteristics. The geographic proximity to the Bering and Chukchi  
81 seas that both have experienced rapid sea ice loss and climatic shifts in recent years offers a unique opportunity to study the  
82 relationship between changing climate regimes and lake dynamics in permafrost regions on short-time-scales. In this study we  
83 therefore use temporally high-resolution remote sensing and meteorological data to quantify:

- 84 1) How much lake area was affected by the recent drainage events in western Alaska in 2018?
- 85 2) How do the drainage events, documented in 2018, compare to other previous events such as in the mid 2000's in  
86 terms of area, spatial distribution, and temporal (intra-annual) sequence?
- 87 3) What are the primary drivers of the recent drainage events and how may projected future climate scenarios affect lake  
88 trajectories in this region?

89 To answer these questions, we analyzed recent optical and synthetic aperture radar (SAR) satellite imagery (Planet, Sentinel-  
90 1) from 2017 and 2018 to map the spatio-temporal lake change dynamics and compared the results to available datasets of past  
91 lake dynamics (Nitze et al., 2018a; Nitze et al., 2018b) and climatic conditions. Furthermore, we investigated weather and  
92 climate data as well as modeled lake ice conditions as potential drivers of the widespread lake drainage.



## 93 2 Study area

94 In this study, we focus on the northern Seward Peninsula (NSP) and the Baldwin Peninsula (BP) in western Alaska. The study  
95 area covers a total land area (including interior water bodies) of 25,271 km<sup>2</sup>. It is bounded by the Chukchi Sea and Kotzebue  
96 Sound to the north and northwest, different hill ranges in the south, and Selawik Lake, Hotham Inlet and the 161°W meridian  
97 in the east (Figure 1). It is part of the Bering Land Bridge region, which was largely unglaciated during the last glacial  
98 maximum and is now located at the southern margin of the continuous permafrost zone (Jorgenson et al., 2008; Obu et al.,  
99 2019). Measured ground temperatures range between -3.5 and -0.8 °C (Biskaborn et al., 2015; GTN-P Ground Temperature  
100 Database). Modeled ground temperatures range between -2.8 and +0.5 °C, with the majority between -1.5 and -2.0°C (Obu et  
101 al., 2019).

102 The area is characterized by a subarctic continental climate with a mean annual air temperature (MAAT) of -5.1 °C and 279  
103 mm precipitation as reported at the Kotzebue climate station (NOAA, 1981-2010). Snowfall accumulation averages 157 cm  
104 per year, considerably more than for example in northern Alaska (~95 cm in Utkiagvik/Barrow). Snow typically persists until  
105 the mid to end of May (Macander et al., 2015).

106 The study region is composed of a strongly degraded ice-rich permafrost landscape with typical permafrost landforms, such  
107 as thermokarst lakes and drained thermokarst lake basins of several generations (Plug and West, 2009; Jones et al., 2011;  
108 Jones et al., 2012), pingos, ice wedge polygon networks, and ice-rich yedoma uplands as remnants of the Pleistocene  
109 accumulation plain (Hopkins et al., 1955; Jongejans et al., 2018). The morphology is variable with mostly flat terrain (<20 m)  
110 in highly degraded permafrost terrain along the coastal margin of the NSP and undulating terrain with steep slopes in the  
111 upland regions of the NSP. The mountainous terrain along the southern margin of the NSP reaches up to ~700 m elevation.  
112 The Baldwin Peninsula (BP) is characterized by rolling terrain from sea-level to ~50 m elevation with a mixture of degraded  
113 permafrost with partially drained lake basins and uplands in various stages of degradation (see Figure 1).

114 The foothills and mountain ranges of the study area are underlain by bedrock. Furthermore, the NSP is locally affected by Late  
115 Quaternary volcanism, with the presence of four known maar lakes (Devil Mountain, White Fish, North Killeak, South  
116 Killeak), which are the largest lakes of the study region and the largest maar lakes globally (Beget et al., 1996). Further volcanic  
117 landscape features such as degraded volcanic bedrock cores, young basaltic lava flows and young cinder cones are locally  
118 present in the southern portion of the NSP (Hopkins, 1955). In part, deposits of the BP are likely of glacial origin, with a buried  
119 terminal moraine covered with yedoma-like, ice-rich sediments (Huston et al., 1990; Jongejans et al., 2018).

120 The region is one of the major lake districts in Alaska (Arp and Jones, 2009). Lake presence in the selected study area is  
121 concentrated on the coastal plains and thermokarst terrain. The majority of lakes are located in drained thermokarst lake basins,  
122 have shallow depths of less than 2 m, and are often later generation thermokarst lakes in locations that experienced several  
123 previous lake generations (Jones et al., 2012; Lenz et al., 2016). However, first generation thermokarst lakes up to 15 m in  
124 depth, intersecting the remaining yedoma upland surfaces, are still present (Kessler et al., 2012). Yedoma uplands with flat



125 surfaces are speckled with initial thermokarst ponds and small lakes, most notably on the BP (Jongejans et al., 2018). In  
126 addition, the four large maar lakes on the NSP that reach depths of up to 100 m (Beget et al., 1996).  
127 Vegetation is predominantly composed of shrubby tundra and is located in zones D and E of the Circumpolar Arctic Vegetation  
128 Map (CAVM) (Walker et al., 2005). Vegetation is typically abundant in sheltered areas along thermokarst lake margins.  
129 Floating vegetation mats may be present on lakes margins and persist above water associated with expanding lake margins  
130 (Parsekian et al., 2011).

### 131 **3 Data and Methods**

#### 132 **3.1 Data**

##### 133 **3.1.1 Lake dataset base layer**

134 We used the lake change dataset of Nitze et al. (2018a, 2018b) as the base layer for further analysis. This dataset contains  
135 polygon vectors of the buffered lake extent of individual lakes larger than 1 ha. It includes spatial attributes and statistics such  
136 as individual lake area in 1999 and 2014, net change (gain minus loss) and gross changes (gain, loss) from 1999-2014, as well  
137 as lake shape parameters, such as orientation, eccentricity, and solidity. All lakes intersecting the study area (n=4605) were  
138 selected for analysis. Further GIS and spatial analyses are based on the geometries of this lake dataset (Lake Change 1999-  
139 2014: named Lk hereafter). An overview of the lake change datasets is provided in Table 1.

#### 140 **3.2 Remote sensing analysis**

##### 141 **3.2.1 Water masks for 2017 and 2018: Sentinel-1 imagery**

142 We extracted late-summer water masks for the years 2017 and 2018 using Sentinel-1A/B SAR data in Google Earth Engine  
143 (GEE) (Gorelick, et al., 2017) (see Figure 2). We identified all Sentinel-1A/B images available between 1 August and 30  
144 September in both 2017 and 2018 (Watermask 2017: WM2017, Watermask 2018: WM2018) and selected VV polarization,  
145 which was available for all S1-data within this period. Erroneous low-backscatter values along image margins, which are a  
146 common issue for these datasets, were clipped per default with a buffer of 5000 m.

147 We created a median value composite of the entire image stack, to lessen the impact of very high backscatter values caused by  
148 windy conditions. After histogram analysis, we determined a backscatter value of -18 dB as the best threshold point between  
149 land and water. All backscatter values below -18 dB were added to the surface water masks of 2017 (WM2017) and 2018  
150 (WM2018), respectively. We exported the two water masks to raster files with 20x20 m grid spacing in UTM3N projection.  
151 The water masks WM2017 and WM2018 were intersected with the lake extent base layer (Lk) using zonal statistics in QGIS  
152 version 3.6 (QGIS Development Team, 2019) to retrieve lake area extent and zonal statistics values for 2017 and 2018.



153 Lastly, all lakes with a lake area loss of >25 % and initial size of >1 ha, based on the difference of WM2017 and WM2018,  
154 were defined as drained lakes. This follows previous studies defining drainage thresholds by lost water area of >25 % (Hinkel  
155 et al., 2007; Olthof et al., 2015; Jones et al., 2020a). The drained lakes dataset is referred to as LkDrain.

156

157 Links to the GEE code used for water masking are provided in the Code and Datasets Section.

### 158 **3.2.2 Timing of drainage 2017 and 2018: Planet imagery**

159 To determine the drainage patterns and mechanics as well as to compare long-term versus short-term drainage patterns, we  
160 automatically analyzed temporally high-resolution Planet CubeSat imagery (Planet Team, 2017) from 2017 and 2018 and  
161 visually inspected the largest drained lakes. With over 120 satellites in orbit, the Planet constellation provides a temporal  
162 frequency of observations of less than one day at a ground resolution of 3.125 m, which makes Planet data an ideal solution  
163 for mapping rapid landscape dynamics at high spatial and temporal resolutions. For mapping individual lake dynamics in 2017  
164 and 2018, we used the automated lake tracking workflow presented in Cooley et al. (2017, 2019). A complete description of  
165 the method can be found in Cooley et al. (2019). A brief summary is provided here. First, we downloaded all PlanetScope  
166 (3.125 m resolution) and RapidEye OrthoTiles (5 m resolution) with <20 % cloud cover available from Planet Labs between  
167 May 1 and October 1 for both 2017 and 2018. We then created an initial lake mask which contains the maximum extent of all  
168 water bodies in the study area between 2017 and 2018. This initial mask was buffered by 60 m and all rivers were removed to  
169 produce a buffered water mask used for both seeding the water classification and tracking changes in lake area.

170 We then classified all of the images into water or land by applying a histogram-derived threshold to each image's NDWI  
171  $((\text{NIR}-\text{green}) / (\text{NIR}+\text{green}))$  as described in Cooley et al. (2017; 2019). To track changes in lake area, we used an object-  
172 based lake tracking method wherein for every image, we calculated the total amount of water contained within each lake object  
173 in the buffered mask. This method allows for direct comparison between RapidEye and PlanetScope imagery with its different  
174 spatial resolution and furthermore is robust against potential minor geolocation uncertainty.

175 At the time of analysis, Planet Labs imagery did not provide a reliable cloud mask. Therefore, the third and most critical step  
176 of the method was removal of cloudy or poor quality observations using a machine learning-derived filtering algorithm. To do  
177 this, we first created a manual training dataset of valid/invalid lake area observations and then used this dataset to build a  
178 random forest classifier that automatically removes cloudy/poor quality lake observations. This method is able to accurately  
179 classify 97 % of observations as valid or invalid. We then selected the best observation for each day and applied additional  
180 outlier and median filters to produce the final time series. While we do not specifically remove ice-covered observations from  
181 the analysis, Cooley et al. (2019) demonstrate that most ice-impacted lake area observations are classified as invalid by the  
182 random forest classifier.



183 The final lake dynamics dataset, henceforth referred to as LkDyn, includes buffered polygon vectors, seasonal time series of  
184 lake area, as well as basic descriptive lake area statistics such as minimum area, maximum area, and seasonal dynamics (max  
185 - min) for each individual lake. For the analysis of temporal lake drainage patterns we spatially joined all lakes of LkDyn,  
186 which intersected LkDrain.

### 187 **3.2.3 Identifying past lake drainage for 1999-2014**

188 For lake dynamics from 1999-2014, we used the lake change dataset of Nitze et al. (2018) (Lk) to compare recent dynamics  
189 to the observed drainage events of 2018. We opted for manual image interpretation based on satellite imagery video animations  
190 as there is to our best knowledge no reliable automated method available to determine drainage dates in challenging Arctic  
191 environments. We tested the automated LandTrendr method, which automatically determines breakpoints in time-series, to  
192 retrieve the timing of lake drainage between 1999 and 2018 (Kennedy et al., 2010; Kennedy et al., 2018). Results obtained  
193 with this method were highly unstable with insufficient reliability.

194 We created video animations in GEE for each individual drained lake, with time-stamped frames, and determined the drainage  
195 year manually through visual interpretation (link to code see below). The drainage year was defined as the point in time of  
196 initial clearly visible drainage, which could be a) visible exposure of lake bottom sediments or b) a strong increase in  
197 vegetation, e.g. due to sudden lake level drop. The entire calculated area loss was assigned to the determined drainage year.  
198 Lake area loss of lakes with a longer drainage process >1 year, e.g. from 2005 until 2009, were counted as full drainage in the  
199 initial drainage year (2005). The visual interpretation was aided by plotting the time-series of multi-spectral indices (Tasselled  
200 Cap, NDVI, NDWI) for each individual drained lake.

201 Lakes with data gaps (up to several years) right before the determined drainage year, were flagged in the statistics. This  
202 frequently applied to years 2005 and 2008, which had several data gaps in the preceding years (see Supplementary Figure 1).  
203 Data gaps were caused by limited data availability, frequent cloud cover and shadows, as well as the Landsat-7 Scan Line  
204 Corrector (SLC) error. Lakes where the timing could not be detected manually, e.g. in case of very subtle drainage, were  
205 assigned no drainage year (25 of 270).

206 Links to the GEE video animation processing code and time-series plotting are provided in the Code and Datasets Section.

207 The videos are accessible at:

208 [https://github.com/initze/NW\\_Alaska\\_Drainage\\_Paper/tree/master/animations/lake\\_animations\\_drainage\\_1999-2014](https://github.com/initze/NW_Alaska_Drainage_Paper/tree/master/animations/lake_animations_drainage_1999-2014)

209

## 210 **3.3 Climate and weather analysis**

### 211 **3.3.1 Weather**

212 We analyzed synoptic weather data from the nearest weather station in Kotzebue that is provided by the National Oceanic and  
213 Atmospheric Administration (NOAA). We acquired the GHCN-Daily datasets (Menne et al., 2012) in CSV format through



214 the web-search on the NOAA website (<https://www.ncdc.noaa.gov/cdo-web/search>). The dataset provides a daily series of  
215 minimum ( $t_{\min}$ ) and maximum ( $t_{\max}$ ) temperatures ( $t$ ), precipitation ( $\text{prcp}$ ) and snowfall ( $\text{sf}$ ) from 1897 until 2019, with  
216 continuous observations since 1950. Daily mean temperatures are not available continuously. Therefore, we calculated daily  
217 mean temperatures as the mean of daily minimum and daily maximum temperatures. For calculating the influence of winter  
218 conditions ( $t$ ,  $\text{prcp}$ ,  $\text{sf}$ ) we analyzed the weather conditions from July 1 of the preceding year until June 30 on a yearly basis,  
219 from here on referred to as “winter year”. Therefore, winter year 2018 for example is defined as the period from July 1 2017  
220 through June 30 2018. In addition to the standard attributes (mentioned above), we calculated Freezing Degree Days (FDD)  
221 as the cumulative sum of negative mean daily temperatures per winter year. Snow accumulation is calculated as the cumulative  
222 sum of snowfall per winter year.

223 We calculated climatological means for daily observations and yearly aggregated statistics. For daily values we calculated  
224 means and standard deviations of mean temperatures ( $t_{\text{mean}}$ ) for each calendar day, excluding 29 February, from 1 January 1981  
225 through 31 December 2010. We calculated yearly mean temperature as the mean of daily  $t_{\text{mean}}$  mean temperatures ( $t_{\text{mean}}$ ). We  
226 calculated the mean of yearly values between 1981 and 2010 as the climatic mean temperature. For annual statistics of winter  
227 years we calculated values ranging from July 1980 through June 2010, according to the previously stated winter year definition.  
228 Code: For climate and weather data preprocessing and time-series plotting, a python package was developed by Ingmar Nitze,  
229 which is available at <https://github.com/initze/naaplotter>.

### 230 **3.3.2 Climate prediction**

231 We downloaded Decadal SNAP (Scenarios Network for Alaska and Arctic Planning, 2020) Ensemble Climate Model  
232 Projections (2 km CMIP/AR5) of Scenarios RCP4.5, RCP6.0, and RCP8.5 for the study region. This dataset contains decadal  
233 (2000-2010, 2010-2020, ..., 2090-2100) mean annual, seasonal and monthly air temperature and precipitation. For analysis  
234 we used annual predictions of temperature (MAAT) and precipitation (MAP). Gridded data is available at a spatial resolution  
235 of 2 km across Alaska and parts of western Canada. We clipped the data to the extent of the study area and calculated the mean  
236 and standard deviations for the entire study region for projected MAAT and MAP values for each decade.

### 237 **3.4 Lake ice simulations**

238 We used the Canadian Lake Ice Model (CLIMo; Duguay et al., 2003) to analyze the impact of weather conditions on lake ice  
239 growth and permafrost. CLIMo is a 1-D thermodynamic ice model that has been used in several studies (Ménard et al., 2002;  
240 Labrecque et al., 2009; Brown and Duguay, 2011; Surdu et al., 2014; Antonova et al., 2016). CLIMo output includes all energy  
241 balance components, on-ice snow depth, the temperature profile at an arbitrary (specified) number of levels within the ice/snow  
242 (or the water temperature if there is no ice) and ice thickness (clear ice and snow ice) on a daily basis, as well as freeze-  
243 up/break-up dates and end-of-season clear (congelation) ice, snow ice and total ice thickness. Model output of particular  
244 interest to lake ice simulations within the context of this study is the evolution of lake ice growth and maximum ice thickness



245 as they are useful proxies for freezing intensity and the influence of weather conditions on potential ground stability.  
246 Thicknesses of snow ice and that of congelation ice layers (referred to hereafter as “top-growth” and “bottom-growth”,  
247 respectively) were also analyzed to account for snow mass and snow insulation effects.  
248 The lake ice model is forced with five meteorological variables consisting of mean daily near-surface air temperature, relative  
249 humidity, wind speed, cloud cover, and snowfall (or snow depth from a nearby land site when available). Four of the five  
250 meteorological variables (all but snowfall) were taken directly or derived from the ERA5 atmospheric reanalysis product from  
251 the European Centre for Medium-Range Weather Forecasts (ECMWF). Since ERA5 did not provide adequate snowfall or  
252 snow depth values, we obtained snow depth data from NOAA’s Global Historical Climate Network Daily (from the nearest  
253 weather station at Kotzebue Ralph Wien Memorial Airport) for model simulations.  
254 We performed simulations over nearly a 40-year period (1980-2018) and with specification of a mixed-layer depth of 2 m.  
255 The length of the record was chosen based on the availability of ERA5 data and to be able to place lake ice model output for  
256 the 2018 winter year into a broader historical context. Finally, in order to account for redistribution of snow across lake ice  
257 surfaces which is a process well documented in several studies (e.g. Duguay et al., 2003; Sturm and Liston, 2003; Brown and  
258 Duguay, 2011; Kheyrollah Pour et al., 2012), we ran the model with two sets of snow depth scenarios; one with full snow  
259 cover (100% of the amount measured at the Kotzebue weather station) and the other with no snow cover (0% snow – i.e. snow  
260 free ice surface) to capture the range of snow conditions that one would expect to observe in the field.

## 261 **4 Results**

### 262 **4.1 Lake changes**

#### 263 **4.1.1 Lake drainage 2018**

264 Lake area loss was severe in 2018, where 192 of 4605 lakes larger than 1 ha lost more than 25 % of their initial size (LkDrain).  
265 These lakes lost an accumulated water area of 1622.04 ha between late summer 2017 and 2018. Total net lake area loss,  
266 including all lakes, was 2062.56 ha (4 % of the total lake area in the study domain).

267 Lake drainage clustered around two types of lake sizes. Five very large lakes (>100 ha) lost 1072.68 or 66.1 % of the total  
268 drained lake area (LkDrain), while the remaining 190 lakes accounted for 549.36 ha or 34.9 %, where the largest lake had an  
269 initial size of 28.5 ha in 2017 (Table 2). Of the five large drained lakes, four are of thermokarst origin and the largest is a  
270 lagoon on the BP, which likely is affected by episodic flooding and drying. The five large lakes that drained were some of the  
271 largest thermokarst lakes in the entire study area before drainage (Size rank 6, 12, 32, 39, 51). The only other bigger lakes in  
272 the study region were formed or affected by Late Quaternary volcanic activity (four maar lakes and Imuruk Lake) and therefore  
273 are less prone to lake drainage caused by permafrost degradation.

274 Spatially, the highest density of lake drainage events is located in the Cape Espenberg region in the northeastern part of the  
275 NSP (see Figure 3). On the BP, two spatial clusters of lake drainage prevail. The first cluster is located in the center of the



276 northern part of the BP, which encompasses the now drained formerly largest lake (Lake ID 64656) and its neighboring basins.  
277 The second cluster is located in the southern part of the BP, where several partially drained lakes form a nearly linear structure.  
278 Smaller clusters or individual lake drainage events are scattered predominantly along coastal and lowland areas of the entire  
279 study region and across different landscape units, such as uplands, thermokarst basins, coastal depressions or river floodplains.  
280 Lake drainage in the southern more mountainous region of the SP was scarce.

#### 281 **4.1.2 Intra-annual lake drainage dynamics**

##### 282 **Temporal Patterns**

283 The analyzed lakes exhibit various distinct seasonal patterns of lake area loss or drainage. The ice-break-up period in late May  
284 and early June 2018 was the most dominant period of lake drainage. Nine of the largest 10 lakes (see Table 3) exhibit a strong  
285 decline in lake area before July 2018, and one rapid drainage event in early July (Lake ID 101359). In the majority of these  
286 cases (n=8), the first valid observation of 2018 already shows a significant decline compared to the last observation of 2017,  
287 which indicates drainage during snow-melt and ice-break-up, when data observations were still masked due to the presence of  
288 ice and snow. During June 2018 weather conditions were favorable for optical remote sensing and observations for ice-free  
289 persistent lakes are available. From July lake area only decreased slowly and gradually among the analyzed lakes (LkDrain)  
290 without further distinct drainage peaks. A detailed example of a representative lake drainage event is presented in Figure 4.  
291 Apart from the general regional dynamics, individual lake drainages followed variable patterns of drainage velocity/duration  
292 and timing. Drainage patterns included sudden complete lake area loss (e.g. Lake IDs 99230, 64656), multiple recurring  
293 drainage events (Lake IDs 72420, 100644, 99583), gradual loss (Lake IDs 99756, 100218) to initial loss followed by partial  
294 refilling (Lake IDs 99381, 99465, 99532) (see Supplementary Files).

295 Supplementary figures are available at:

296 [https://github.com/initze/NW\\_Alaska\\_Drainage\\_Paper/tree/master/figures/lake\\_drainage/planet\\_lake\\_area](https://github.com/initze/NW_Alaska_Drainage_Paper/tree/master/figures/lake_drainage/planet_lake_area)

297

##### 298 **Quantification**

299 The early season lake drainage affected the largest lakes, and therefore the largest area. The time-series animation of the ten  
300 largest lakes can be accessed by video (see Table 2). The third largest drained lake (Lake ID 99230) for example started  
301 draining on June 2 and lost the majority of its water within the following two weeks. During the summer months the remaining  
302 shallow ponds dried out further, while only few apparently deeper ponds remained. Imagery from spring 2019 showed the  
303 development of vegetation, which follows the typical thermokarst lake cycle of this region (lake, lake drainage, drying of  
304 exposed lake bottom, vegetation emergence; Jones et al., 2012) (see Table 2 for video). The largest drained lakes follow a  
305 similar trajectory of rapid drainage around ice-break-up and further drying of the drained lake basin during peak summer.



306

### 307 **Spatial patterns**

308 Nine out of the ten largest drained lakes are second generation thermokarst lakes, which are typically located within a complex  
309 of previously drained lake basins. The second largest “lake” is actually a lagoon, which is likely influenced by sea water  
310 inundation. Each of the lakes had a significant fraction of their shoreline within the former drained lake basin. These are  
311 typically covered by wet tundra and underlain by terrestrial peat overlying lacustrine sediments (Jones et al., 2012). Based on  
312 visual image interpretation, all lakes drained through previously established drainage pathways, which are located in flat basin  
313 terrain and suggest that these likely are “weak spots” for full drainage.

314 During these drainage events new channels formed or existing channels deepened. In several instances (Lake IDs 99368,  
315 64656, 99492, 102499), new drainage channels are evident based on new sediment fans that formed downstream. In the case  
316 of several lakes, the drainage caused a chain reaction, where hydrologically connected lakes, both up- and/or downstream of  
317 the initially drained lake, drained as well. Due to the widespread presence of these surface drainage indicators, talik penetration  
318 to a groundwater layer can be excluded for the study area.

### 319 **4.1.3 Lake drainage 1999-2014**

320 From 1999 through 2014 we observed 268 lakes larger than 1 ha that lost more than 25 % of their area, resulting in a total  
321 water area loss of 3245.74 ha during the observed period within this group of lakes. The net lake loss of the study region,  
322 including all lakes was 3677.43 ha or 6.0 % of the overall lake area. The six largest drained lakes accounted for more than half  
323 of the lost lake area (50.6 %) and were each among the 33 largest lakes (Size rank 9, 12, 13, 26, 29, 33) of the study area (Table  
324 3). Each of these lakes was apparently of thermokarst origin.

325 These drained and partially drained lakes predominantly occur along the near coastal zone of the NSP and around Shishmaref  
326 Inlet (see Figure 3). Within this region, lake drainages are distributed uniformly with no distinct clusters. The BP and southern  
327 Kotzebue Sound do not show major drainage activity in this period with only three lakes that fulfill the defined criteria. The  
328 vicinity of Imuruk Lake had four drained lakes.

329

### 330 **Timing of drainage**

331 The analysis of drained lakes revealed a period of widespread lake drainage with up to 21 confirmed events per year from  
332 2002 until 2007 and 2009 (see Supplementary Figure 2). The number of detected drained lakes in 2005 was exceptionally high  
333 with 56, but the majority (n=33) did not have sufficient observations in the preceding year 2004 or even 2003 to confirm the  
334 correct drainage year. This number of drained lakes is therefore associated with a high degree of uncertainty. Years 2003,  
335 2007, 2009 and 2012 also have more than 5 lakes, which have an uncertain drainage date.

336 Although the number of drained lakes is relatively stable over time, drained lake area spiked in 2006 and 2007 with 922 ha  
337 (uncertain: 6.35 ha) and 631 ha (uncertain: 15.57 ha) net lake area loss, respectively. The significant uptick in 2006 was driven



338 by the drainage of very large lakes, particularly in the Cape Espenberg region of the NSP. The years 2003 and 2004 follow  
339 with lake area loss of 323.65 ha (uncertain: 41.58 ha) and 413.06 ha (uncertain: 3.91 ha), respectively. The numbers are  
340 conservative and might be even higher (see uncertainty 2005) due to a low data coverage during this period.

## 341 **4.2 Weather and Climate**

### 342 **4.2.1 Weather observations**

343 The preceding winter and spring of 2017/2018 (winter year 2018) was the warmest, wettest and second snowiest on record at  
344 this time. Compared to the entire weather record this winter was highly exceptional (Figure 5, Table 4). Mean daily air  
345 temperatures exceeded the climatological means persistently and frequently with 127 days above one standard deviation from  
346 the climatological mean, only interrupted by a short cold snap in January 2018 (Figure 6). On several days air temperatures  
347 were close to 0 °C, which is 15 to 20 °C above the climatological mean. Exceptional warmth lasted continuously from October  
348 2017 until fall 2019. Winter year 2019 even surpassed 2018 with an annual air temperature of +0.12 °C, but with average  
349 precipitation and snowfall accumulation of 279 mm and 155 cm, respectively.

350 The weather station recorded only 1905 cumulative Freezing Degree Days (FDD; the sum of average daily degrees below 0  
351 °C) and an annual air temperature of -1.3 °C, which exceeded the previous record by 0.53 °C and 238 FDD. The 10 warmest  
352 and 5 coldest years are shown in Table 5. Accumulated snowfall was the 2<sup>nd</sup> highest on record with 274 cm, only exceeded by  
353 2005 (305 cm). Overall precipitation of the winter year 2018 was the highest on record with 424.5 mm, exceeding very wet,  
354 but much colder winter years 2013 (402 mm, -5.41 °C) and 1995 (393.7, -5.92°C). Precipitation, mostly as snowfall, was  
355 particularly strong from October through February, with the exception of January.

356 All indicators highlight the exceptional conditions of winter 2017/2018 in western Alaska. Weather data from Nome (ca. 300  
357 km south of Kotzebue) on the southern SP indicate a similar picture of extreme weather conditions with the second warmest  
358 and third-snowiest winter year on record. Climate reanalysis data (GHCNv4) confirm a larger regional pattern of exceptionally  
359 warm conditions across the Bering Strait (see Supplementary Figure 2).

### 360 **4.2.2 Climate model projections**

361 The UAF SNAP Climate model ensemble consistently projects an increase in temperature and precipitation for western Alaska  
362 with a plateau after around 2070 for RCP4.5 and continuous increase for the remaining scenarios in the 21<sup>st</sup> century. They  
363 predict an increase to a regional MAAT of  $-0.39 \pm 0.38^{\circ}\text{C}$  (RCP4.5),  $+0.44 \pm 0.37^{\circ}\text{C}$  (RCP6.0), and  $+3.00 \pm 0.38^{\circ}\text{C}$  (RCP8.5)  
364 during the 2090s, which marks an increase of 3.7 to 6.6 °C (Supplementary Figure 3). MAP is projected to increase by around  
365 12 % (RCP4.5), 20 % (RCP6.0), and 32 % (RCP8.5) on average.



### 366 **4.3 Lake ice simulations**

367 Modeled maximum lake ice thickness of the winter year 2018 was 1.14 (100% snow) to 1.32 m (no snow). It was below  
368 average compared to 1981-2017 ( $1.31 \text{ m} \pm 0.14 \text{ m}$  for 100% snow;  $1.68 \text{ m} \pm 0.12 \text{ m}$  for no snow) but thicker than the absolute  
369 minimum of 0.99 m (100% snow) in 2014. Lake ice thickness of 2018 was primarily determined by top ice-growth (snow-ice  
370 formation), which is strongly dependent on snow mass on the ice surface. Snow-ice formation correlates well with high  
371 snowfall years, such as 2005 or 2011. The bottom (congelation) ice-growth of 2018 reached a new extreme low with only 0.32  
372 m (100% snow) to 1.32 m (no snow) (see Figure 7). This compares to  $0.87 \text{ m} \pm 0.23 \text{ m}$  (100% snow) and  $1.68 \text{ m} \pm 0.12 \text{ m}$  (no  
373 snow) from 1981-2017. Low bottom ice-growth indicates a strongly decreased freezing activity (negative heat flux) into the  
374 lake and potentially into the ground of the surrounding terrain. The exceptional combination of high temperatures and high  
375 snowfall, as experienced in ice season 2017-2018, are the strongest factors for these patterns.

## 376 **5 Discussion**

### 377 **Lake drainage in western Alaska in historical context**

378 The massive drainage of many lakes in early summer 2018 in western Alaska was an extreme event, which dwarfs previous  
379 lake drainage events within this region since the availability of remote sensing data. Although the study area experienced  
380 widespread lake drainage during the mid 2000's (Jones et al., 2011, Nitze et al., 2018a; Swanson, 2019), the year 2018  
381 exceeded average annual lake drainage rates of 1999-2014 by a factor of 7.5 in area and 10.9 in numbers of lakes, clearly  
382 indicating a response of the system to extreme weather conditions. Recent lake drainage in 2018 even doubled the previous  
383 record year of 2006 in drained area and 10-fold in number of drained lakes. From 1950 until 2006/2007 lake drainage and lake  
384 expansion rates on the northern SP were fairly stable. The strong influence of large lakes on drainage rates in 2018 confirmed  
385 previous findings (Jones et al., 2011). A recent study by Swanson (2019) identified the same exceptional event for the National  
386 Parks of northwestern Alaska, which partially overlaps with our study area.

387 The high level of degradation, apparent by a large fraction of drained basins of several generations (Jones et al., 2012; Regmi  
388 et al., 2012), shows the general susceptibility of the landscape to rapid thermokarst lake dynamics, including drainage, within  
389 the study region. This landscape underwent intense thermokarst development over the past millennia, with the onset of  
390 thermokarst development during the early Holocene (Wetterich et al., 2012; Farquharson et al., 2016; Lenz et al., 2016).  
391 Available data of historic lake drainage is sparse. Therefore, a comparison of recent drainage rates with long-term development  
392 is difficult due to a lack of consistent observations, in particular for the pre-remote-sensing period.

### 394 **Local context**

395 The BP stands out in particular with a strong increase in lake drainage events in 2018, including its largest lake, relative to the  
396 period of 1999 to 2014. However, as evidenced by newly forming and expanding ponds, which are dotting the landscape,



397 active thermokarst lake expansion prevailed during the preceding decades, but rarely triggered drainage events. A recent study  
398 by Jones et al. (2020b) has found a significant expansion of beaver dam building activities on the Baldwin Peninsula. Beavers  
399 strongly influence local hydrological regimes by damming up thermo-erosional valleys or drained lake basins, which leads to  
400 pond and lake formation and could potentially factor into lake drainage dynamics.

401 On the SP lake drainage was concentrated on the coastal region, particularly the Cape Espenberg lowlands, which are also hot-  
402 spots of previous lake drainage events of the past decades. The location of recently drained lakes follows patterns of strong  
403 Holocene thermokarst activity (Lenz et al, 2016) in the same area, which is apparent in highly degraded surface morphology.

#### 404 **Influencing factors**

405 The exceptional weather conditions in western Alaska are likely the main cause of the significant lake drainage events of  
406 summer 2018. Abundant snowfall with the second highest cumulative snowfall on record created a thicker-than-usual  
407 insulation layer for the ground, which kept cold winter temperatures from penetrating the ground. This situation in combination  
408 with record high winter temperatures, often just below freezing, likely led to an unfavorable energy balance for the stability of  
409 permafrost. Both snow cover (Stieglitz et al., 2003, Ling and Zhang, 2003; Osterkamp, 2007) and winter temperatures are  
410 important factors for near surface permafrost conditions. The abundant early winter snowfall in October and November in our  
411 study area further increased the already strong snow insulation effect (Ling and Zhang, 2003).

412 The severe combination of both negative influencing factors very likely restricted the refreezing of the active layer and thus  
413 potentially caused a landscape-wide talik development between the active layer and permafrost in 2018. Thinning of lake ice  
414 during the ice growth season, also due to increased snow depth and warmer winter temperatures, has been identified as a factor  
415 responsible for the shift from bedfast ice to floating ice on shallow lakes in several regions and to formation of new taliks  
416 underneath lakes that previously were underlain by permafrost on the Alaska North Slope (Surdu et al., 2014; Arp et al., 2016;  
417 Engram et al., 2018). In addition, later freeze-up in the fall period leads to a longer exposure of the near-shore lake-bed to  
418 water, which likely increases permafrost destabilization and talik formation or growth along shores. Reports from Fairbanks  
419 in interior Alaska, with a similar pattern of mild and snow-rich winter weather conditions, show that at various sites the active  
420 layer did not refreeze completely during winter 2017/2018 (Farquharson et al., 2019b). The recent movement of beavers from  
421 the treeline to tundra regions in northwestern Alaska could also be a contributing lake drainage mechanism that requires further  
422 attention (Tape et al., 2018; Jones et al, 2020b).

423

#### 424 **Temporal sequence and causes**

425 The occurrence of lake drainage around (during or shortly after) ice break-up indicates drainage driven by bank overtopping  
426 or breaching in combination with rapid thermo-erosion during outflow. High water levels due to high precipitation in fall and  
427 winter, rapid melt of abundant snow, in combination with destabilized lake margins, and possible talik formation have very  
428 likely led to bank overflow or breaching of lake shores, and subsequent thermo-erosion and deepening of outflow channels.  
429 The location of lakes within older drained lake basins with comparably unstable peaty and fine-grained substrates with high



430 intra-sedimentary ground ice contents as well as ice wedge networks enhanced the susceptibility of lakes to erosion and  
431 drainage in addition to the weather induced driver.

432 Under current weather/climatic conditions with a MAAT around 0 °C, 5 °C above normal (1981-2010), permafrost aggradation  
433 in the freshly exposed lake-beds might be slowed or even prevented, with consequences for basin hydrology and  
434 biogeochemical cycling. After lake drainage, the lake-bed typically refreezes and permafrost soils can redevelop, which locks  
435 in carbon stored in lacustrine sediments and terrestrial peat (Walter Anthony et al., 2014). *In-situ* measurements and continued  
436 observations are necessary to test this hypothesis and determine whether this is happening already now on the SP and BP.

437

### 438 **Spatial comparison and considerations**

439 Western Alaska has been previously identified as one of the regions with the most intensive lake dynamics on a decadal-scale  
440 (Nitze et al., 2017; Nitze et al., 2018a; Jones, et al.; 2011; Swanson, 2019; Jones et al., 2020b). Other regions along the  
441 boundary of continuous permafrost in interior Alaska (Chen et al., 2014; Roach et al., 2013; Cooley et al., 2019) or the southern  
442 Yamal Peninsula or western Siberia (Nitze et al., 2018a; Smith et al., 2003) are also highly affected by strong lake dynamics,  
443 too, most notably lake drainage. Lake drainage is a common process in continuous permafrost of colder climates such as the  
444 Arctic coastal plain of Alaska (Hinkel et al., 2007; Nitze et al., 2017; Jones et al., 2020a), Tuktoyaktuk Peninsula (Plug et al.,  
445 2008; Olthof et al., 2015), Old Crow Flats (Labrecque et al., 2009; Lantz and Turner, 2015) or the Kolyma lowlands (Nitze et  
446 al., 2017). However, lake dynamics tend to be of higher magnitude in warmer permafrost regions (Nitze et al., 2018a). In this  
447 context, the drainage event of summer 2018 in our study region in western Alaska exceeded the average extent of lake area  
448 loss by a factor of 7.5 and the previously most extreme year by 2.

449

### 450 **Data quality discussion**

451 The application of different methods and sensors, different temporal scales and varying spatial resolutions (long-term Landsat  
452 datasets vs. Sentinel-1 water masks vs. Planet multi-temporal water masks) may introduce minor differences in masking water  
453 and the delineation of water bodies. In a long-tailed distribution, as observed here, the widely used threshold of >25 % lake  
454 area loss, strongly influences the number of drained lakes. For example, a threshold of >20 % lake area loss leads to an increase  
455 from 192 to 279 drained lakes. However, the influence of total lake area loss remains low.

456 Due to the presence of lake-ice, the automated intra-annual lake tracking algorithm did not detect the early drainage events  
457 reliably, however, the integration of multi-annual data into one analysis will highly benefit the automated lake tracking. With  
458 the exponential growth of available data due to new satellite constellations (Sentinel-1, Sentinel-2, Planet), processing  
459 platforms, and techniques, more reliable, better comparable, and spatially more extensive lake extent datasets will likely  
460 become available in the near future.

461



462 **Outlook**

463 Extreme weather conditions of the winter year 2018 in western Alaska were driven by massively reduced sea ice cover in the  
464 Bering and Chukchi seas, resulting in much warmer and moister weather conditions than usual, which may have caused a so  
465 far unprecedented spatial and temporal clustering of lake drainage event in our study region. As climate models all predict a  
466 significant increase in both mean annual air temperature and precipitation for northern and western Alaska, the dramatic lake  
467 dynamics described here provide an early glimpse of the potentially massive changes in hydrology, permafrost, and topography  
468 to be expected in a warmer Arctic in similarly ice-rich permafrost landscapes. With MAAT around 0 °C, the years 2017 to  
469 2019 already matched the MAAT projected for this region in ~2060 (RCP8.5) to beyond 2100 (RCP4.5) and precipitation  
470 projections for ~2080 (RCP8.5). This mismatch indicates that local to regional permafrost landscapes may experience much  
471 more severe and earlier impacts in a warming Arctic than what climate models are capable of predicting at fine scales.  
472 Permafrost degradation in northern Canada shows that drastic changes in the Arctic climate system can lead to processes which  
473 were projected to happen several decades later (Farquharson et al., 2019a).  
474 The recent events potentially show the fate of lake-rich landscapes in continuous permafrost along its current southern margins,  
475 where near-surface permafrost degradation accelerates and permafrost will become discontinuous in the next decades. The  
476 colder less dynamic lake-rich coastal plain of northern Alaska may become more dynamic once climatic patterns will have  
477 moved towards the middle-to-end of the century.

478 **6 Conclusion**

479 The lake-rich northern Seward and Baldwin peninsulas in northwestern Alaska were affected by unprecedented lake drainage  
480 in 2018, which dwarfed previous lake changes of this historically dynamic permafrost landscape. Due to the mean annual air  
481 temperatures of this region reaching values close to 0 °C in combination with exceptional precipitation in recent years,  
482 matching model projections for the years 2060 (RCP8.5) to 2100 (RCP4.5), near-surface permafrost is likely already in a phase  
483 of degradation and destabilization around the lake margins. This in combination with rapid availability of excess surface water  
484 likely caused the rapid drainage of nearly 200 lakes during or shortly after ice-break up in 2018, including some of the largest  
485 lakes of the region that likely persisted for several millennia. Under a rapidly warming and wetting climate, in conjunction  
486 with ongoing sea ice loss in the Bering Strait, we expect a further intensification of permafrost degradation, reshaping the  
487 landscape and a transition from continuous to discontinuous permafrost, and significant changes in hydrology and ecology.  
488 The impact on habitat and landscape characteristics will be drastic in these formerly lake-rich regions. The recent processes  
489 observed in northwestern Alaska potentially will be a precedent for lake dynamics of rapidly warming lake-rich permafrost  
490 landscapes approaching the MAAT threshold of 0 °C.



491 **Competing Interests**

492 The authors declare that there are no competing interests.

493 **Code and Data**

494 **Data**

495 Supplementary figures and tables data can be found in the supplementary file.

496 **Lake datasets:**

497 [https://github.com/initze/NW\\_Alaska\\_Drainage\\_Paper/tree/master/figures/lake\\_datasets](https://github.com/initze/NW_Alaska_Drainage_Paper/tree/master/figures/lake_datasets)

498

499 **Intra-annual lake area plots:**

500 [https://github.com/initze/NW\\_Alaska\\_Drainage\\_Paper/tree/master/figures/lake\\_drainage/planet\\_lake\\_area](https://github.com/initze/NW_Alaska_Drainage_Paper/tree/master/figures/lake_drainage/planet_lake_area)

501

502 **Weather and climate plots:**

503 [https://github.com/initze/NW\\_Alaska\\_Drainage\\_Paper/tree/master/figures/weather\\_and\\_climate/](https://github.com/initze/NW_Alaska_Drainage_Paper/tree/master/figures/weather_and_climate/)

504

505 **Lake drainage animations:**

506 [https://github.com/initze/NW\\_Alaska\\_Drainage\\_Paper/animations/lake\\_animations\\_drainage\\_1999-2014/](https://github.com/initze/NW_Alaska_Drainage_Paper/animations/lake_animations_drainage_1999-2014/)

507

508 Final lake change datasets will be published on the PANGAEA data repository

509

510 **Code**

511 **Sentinel-1 Watermasks Google Earthengine Script:**

512 <https://code.earthengine.google.com/7d2367758eead1614202efcfa6bed2b5>

513 **Landsat Video Animation Google Earthengine Script:**

514 <https://code.earthengine.google.com/c879add607322305b8293904bea6d781>

515 **noaaplotter weather plotting package:**

516 <https://github.com/initze/noaaplotter>



## 517 Acknowledgements

518 IN and GG were supported by ERC PETA-CARB (#338335), ESA GlobPermafrost, ESA CCI+ Permafrost, and HGF AI-  
519 CORE. BMJ was supported by the National Science Foundation awards OPP-1806213. SC was supported by a National  
520 Science Foundation Graduate Research Fellowship. CD was supported by the Natural Sciences and Engineering Research  
521 Council of Canada (NSERC) grant number RGPIN-05049-2017.

522 We acknowledge help during field work by J. Lenz, M. Fuchs, and J. Strauss.

## 523 References

- 524 Alexeev, V. A., Arp, C. D., Jones, B. M., and Cai, L.: Arctic sea ice decline contributes to thinning lake ice trend in northern Alaska,  
525 *Environ. Res. Lett.*, 11(7), 074022, doi:10.1088/1748-9326/11/7/074022, 2016.
- 526 Antonova, S., Duguay, C., Kääh, A., Heim, B., Langer, M., Westermann, S., and Boike, J.: Monitoring Bedfast Ice and Ice Phenology in  
527 Lakes of the Lena River Delta Using TerraSAR-X Backscatter and Coherence Time Series, *Remote Sens.*, 8(11), 903,  
528 doi:10.3390/rs8110903, 2016.
- 529 Arp, C.D., Jones, B.M.: Geography of Alaska Lake Districts: Identification, description, and analysis of lake-rich regions of a diverse and  
530 dynamic state. U.S. Geological Survey Scientific Investigations Report 2008-5215, 40, 2009.
- 531 Arp, C. D., Jones, B. M., Grosse, G., Bondurant, A. C., Romanovsky, V. E., Hinkel, K. M., and Parsekian, A. D.: Threshold sensitivity of  
532 shallow Arctic lakes and sublake permafrost to changing winter climate, *Geophys. Res. Lett.*, 43(12), 6358–6365,  
533 doi:10.1002/2016gl068506, 2016.
- 534 Arp, C.D., Jones, B.M., Engram, M., Alexeev, V.A., Cai, L., Parsekian, A., Hinkel, K., Bondurant, A.C. and Creighton, A.: Contrasting  
535 lake ice responses to winter climate indicate future variability and trends on the Alaskan Arctic Coastal Plain. *Environ. Res. Lett.*, 13(12),  
536 p.125001, 2018.
- 537 Arp, C. D., Whitman, M. S., Jones, B. M., Nigro, D. A., Alexeev, V. A., Gädeke, A., Fritz, S., Daanen, R., Liljedahl, A. K., Adams, F. J.,  
538 Gaglioti, B. V., Grosse, G., Heim, K. C., Beaver, J. R., Cai, L., Engram, M., and Uher-Koch, H. R.: Ice roads through lake-rich Arctic  
539 watersheds: Integrating climate uncertainty and freshwater habitat responses into adaptive management, *Arct., Antarct., Alp. Res.*, 51(1),  
540 9–23, doi:10.1080/15230430.2018.1560839, 2019.
- 541 Begét, J. E., Hopkins, D. M., and Charron, S. D.: The Largest Known Maars on Earth, Seward Peninsula, Northwest Alaska, *ARCTIC*,  
542 49(1), doi:10.14430/arctic1184, 1996.
- 543 Biskaborn, B. K., -P. Lanckman, J., Lantuit, H., Elger, K., Streletskiy, D. A., Cable, W. L., and Romanovsky, V. E.: The new database of  
544 the Global Terrestrial Network for Permafrost (GTN-P), *Earth Syst. Sci. Data*, 7(2), 245–259, doi:10.5194/essd-7-245-2015, 2015.
- 545 Biskaborn, B. K., Smith, S. L., Noetzli, J., Matthes, H., Vieira, G., Streletskiy, D. A., Schoeneich, P., Romanovsky, V. E., Lewkowicz, A.  
546 G., Abramov, A., Allard, M., Boike, J., Cable, W. L., Christiansen, H. H., Delaloye, R., Diekmann, B., Drozdov, D., Etzelmüller, B.,  
547 Grosse, G., Guglielmin, M., Ingeman-Nielsen, T., Isaksen, K., Ishikawa, M., Johannsson, M., Johannsson, H., Joo, A., Kaverin, D.,  
548 Kholodov, A., Konstantinov, P., Kröger, T., Lambiel, C., Lanckman, J.-P., Luo, D., Malkova, G., Meiklejohn, I., Moskalenko, N., Oliva,  
549 M., Phillips, M., Ramos, M., Sannel, A. B. K., Sergeev, D., Seybold, C., Skryabin, P., Vasiliev, A., Wu, Q., Yoshikawa, K., Zheleznyak,  
550 M., and Lantuit, H.: Permafrost is warming at a global scale, *Nat. Commun.*, 10(1), 264, 2019.
- 551 Bhatt, U.S., Walker, D.A., Walsh, J.E., Carmack, E.C., Frey, K.E., Meier, W.N., Moore, S.E., Parmentier, F.-J.W., Post, E., Romanovsky,  
552 V.E., and Simpson, W.R.: Implications of Arctic Sea Ice Decline for the Earth System. *Annual Review of Environment and Resources* 39,  
553 57-89, 2014.
- 554



- 555 Brown, L.C. and Duguay, C.R.: The fate of lake ice in the North American Arctic. *The Cryosphere*, 5: 869-892, doi:10.5194/tc-5-869-2011,  
556 2011.
- 557 Chambers, M., White, D., Busey, R., Hinzman, L., Alessa, L., and Kliskey, A.: Potential impacts of a changing Arctic on community water  
558 sources on the Seward Peninsula, Alaska. *J. Geophys. Res.* 112, G04S52, 2007.
- 559 Chen, M., Rowland, J.C., Wilson, C.J., Altmann, G.L., and Brumby, S.P.: Temporal and spatial pattern of thermokarst lake area changes at  
560 Yukon Flats, Alaska. *Hydrol. Process.*, 28(3), 837-852, 2014.
- 561 Cooley, S., Smith, L., Stepan, L., and Mascaro, J.: Tracking dynamic northern surface water changes with high-frequency planet CubeSat  
562 imagery. *Remote Sens.*, 9(12), 1306., 2017.
- 563 Cooley, S.W., Smith, L.C., Ryan, J.C., Pitcher, L.H., Pavelsky, T.M.: Arctic-Boreal lake dynamics revealed using CubeSat imagery.  
564 *Geophys. Res. Lett.* 46, 2111-2120, 2019.
- 565 Duguay, C. R., Flato, G. M., Jeffries, M. O., Ménard, P., Morris, K., and Rouse, W. R.: Ice-cover variability on shallow lakes at high  
566 latitudes: model simulations and observations. *Hydrol. Process.*, 17(17), 3465-3483, 2003.
- 567 Elberling, B., Michelsen, A., Schädel, C., Schuur, E.A.G., Christiansen, H.H., Berg, L., Tamstorf, M.P., and Sigsgaard, C.: Long-term CO<sub>2</sub>  
568 production following permafrost thaw. *Nat. Clim. Chang.* 3, 890-894, 2013.
- 569 Engram, M., Arp, C.D., Jones, B.M., Ajadi, O.A., and Meyer, F.J.. Analyzing floating and bedfast lake ice regimes across Arctic Alaska  
570 using 25 years of space-borne SAR imagery. *Remote Sens. Environ.*, 209, 660-676, 2018.
- 571 Farquharson, L.M., Walter Anthony K.M., Bigelow N.H., Edwards M.E., and Grosse G.: Facies analysis of yedoma thermokarst lakes on  
572 the northern Seward Peninsula, Alaska. *Sedimentary Geology*, 340: 25-37. doi: 10.1016/j.sedgeo.2016.01.002, 2016.
- 573 Farquharson, L.M., Romanovsky, V.E., Cable, W.L., Walker, D.A., Kokelj, S., and Nicolsky, D.: Climate change drives widespread and  
574 rapid thermokarst development in very cold permafrost in the Canadian High Arctic. *Geophys. Res. Lett.*, 2019a.
- 575 Farquharson, L. M.; Romanovsky, V. E.; Kholodov, A. L.; Nicolsky, D.; Cable, W.; Walker, D. A., and Kokelj, S. V.: Long-term monitoring  
576 of permafrost degradation documents two forms of landscape response, in: Proceedings of AGU Fall meeting, San Francisco, USA, 9–13  
577 December 2019, abstract #C22C-03, 2019b.
- 578 Gorelick, N., Hancher, M., Dixon, M., Ilyushchenko, S., Thau, D., and Moore, R.: Google Earth Engine: Planetary-scale geospatial analysis  
579 for everyone. *Remote Sens. Environ.*, 202, 18-27, 2017.
- 580 Grosse, G., Jones, B.M., and Arp, C.D.: Thermokarst lakes, drainage, and drained basins, 2013
- 581 GTN-P Ground Temperature Database: <http://gtnpdatabase.org/boreholes>, last access: 30 September 2019.
- 582 Hinkel, K.M., Jones, B.M., Eisner, W.R., Cuomo, C.J., Beck, R.A., and Frohn, R.: Methods to assess natural and anthropogenic thaw lake  
583 drainage on the western Arctic coastal plain of northern Alaska. *Journal of Geophysical Research: Earth Surface*, 112(F2), 2007.
- 584 Hjort, J., Karjalainen, O., Aalto, J., Westermann, S., Romanovsky, V.E., Nelson, F.E., Eitzelmüller, B., and Luoto, M.: Degrading permafrost  
585 puts Arctic infrastructure at risk by mid-century. *Nat. Commun.*, 9(1), 5147, 2018.
- 586 Hopkins, D.M.: Permafrost and ground water in Alaska. US Government Printing Office, 1955.
- 587 Huston, M.M., Brigham-Grette, J., and Hopkins, D.M.: Paleogeographic significance of middle Pleistocene glaciomarine deposits on  
588 Baldwin Peninsula, northwest Alaska. *Ann. Glaciol.*, 14.,111-114, 1990.
- 589 Jones, B.M., Grosse, G.D.A.C., Arp, C.D., Jones, M.C., Walter Anthony, K., and Romanovsky, V.E.: Modern thermokarst lake dynamics in  
590 the continuous permafrost zone, northern Seward Peninsula, Alaska. *Journal of Geophysical Research: Biogeosciences*, 116(G2), 2011.



- 591 Jones, B.M., C.D. Arp, G. Grosse, I. Nitze, M.J. Lara, M.S. Whitman, L.M. Farquharson, M. Kanevskiy, A.D. Parsekian, A.L. Breen, N.  
592 Ohara, R.C. Rangel, and K.M. Hinkel: Identifying historic and future potential lake drainage events on the western Arctic Coastal Plain of  
593 northern Alaska. *Permafrost Periglacial Process*. DOI: 10.1002/ppp.2038, 2020a.
- 594 Jones, B.M., K.D. Tape, J.A. Clark., I. Nitze, G. Grosse, and J. Disbrow: Increase in beaver dams controls surface water and thermokarst  
595 dynamics in an Arctic tundra region, Baldwin Peninsula, northwestern Alaska. *Environ. Res. Lett.*,  
596 <https://iopscience.iop.org/article/10.1088/1748-9326/ab80f1/meta>, 2020b.
- 597 Jones, M.C., Grosse, G., Jones, B.M., and Walter Anthony, K.: Peat accumulation in drained thermokarst lake basins in continuous, ice-rich  
598 permafrost, northern Seward Peninsula, Alaska. *Journal of Geophysical Research: Biogeosciences*, 117(G2), 2012.
- 599 Jongejans, L.L., Strauss, J., Lenz, J., Peterse, F., Mangelsdorf, K., Fuchs, M., and Grosse, G.: Organic matter characteristics in yedoma and  
600 thermokarst deposits on Baldwin Peninsula, west Alaska. *Biogeosciences*, 15(20), 6033-6048, 2018.
- 601 Jorgenson, M.T., Yoshikawa, K., Kanevskiy, M., Shur, Y., Romanovsky, V., Marchenko, S., Grosse, G., Brown, J., and Jones, B.: Permafrost  
602 characteristics of Alaska. In *Proceedings of the Ninth International Conference on Permafrost (Vol. 29, 121-122)*. University of Alaska:  
603 Fairbanks, 2008.
- 604 Karlsson, J.M., Lyon, S.W., and Destouni, G.: Thermokarst lake, hydrological flow and water balance indicators of permafrost change in  
605 Western Siberia. *J. Hydrol.*, 464–465, 459-466, 2012.
- 606 Karlsson, J.M., Lyon, S.W., and Destouni, G.: Temporal behavior of lake size-distribution in a thawing permafrost landscape in northwestern  
607 Siberia. *Remote Sens.*, 6(1), 621-636, 2014.
- 608 Kessler, M.A., L. Plug, and Walter Anthony, K.: Simulating the decadal to millennial scale dynamics of morphology and sequestered carbon  
609 mobilization of two thermokarst lakes in N.W. Alaska, *J. Geophys. Res.*, 117, doi:10.1029/2011JG001796, 2012.
- 610 Kennedy, R. E., Yang, Z., and Cohen, W. B.: Detecting trends in forest disturbance and recovery using yearly Landsat time series: 1.  
611 LandTrendr—Temporal segmentation algorithms. *Remote Sens. Environ.*, 114(12), 2897-2910, 2010.
- 612 Kennedy, R., Yang, Z., Gorelick, N., Braaten, J., Cavalcante, L., Cohen, W., and Healey, S.. Implementation of the LandTrendr Algorithm  
613 on Google Earth Engine. *Remote Sens.*, 10(5), p.691, 2018.
- 614 Kheyrollah Pour, H., Duguay, C. R., Martynov, A., and Brown, L. C.: Simulation of surface temperature and ice cover of large northern  
615 lakes with 1-D models: a comparison with MODIS satellite data and in situ measurements. *Tellus A: Dynamic Meteorology and  
616 Oceanography*, 64(1), 17614, 2012.
- 617 Kravtsova, V.I. and Bystrova, A.G.: Changes in thermokarst lake size in different regions of Russia for the last 30 years. *Kriosfera Zemli*,  
618 13, 16-26, 2009.
- 619 Labrecque, S., Lacelle, D., Duguay, C.R., Lauriol, B., and Hawkings, J.: Contemporary (1951–2001) evolution of lakes in the Old Crow  
620 Basin, northern Yukon, Canada: remote sensing, numerical modeling, and stable isotope analysis. *Arctic*, 62(2), 225-238, 2009.
- 621 Lantz, T.C. and Turner, K.W.: Changes in lake area in response to thermokarst processes and climate in Old Crow Flats, Yukon. *Journal of  
622 Geophysical Research: Biogeosciences*, 120, 513-524, 2015.
- 623 Lenz, J., Grosse, G., Jones, B.M., Walter Anthony, K.M., Bobrov, A., Wulf, S., Wetterich, S.: Mid-Wisconsin to Holocene Permafrost and  
624 Landscape Dynamics based on a Drained Lake Basin Core from the Northern Seward Peninsula, Northwest Alaska. *Permafrost Periglacial  
625 Process.*, 27, 56-75, 2016.
- 626 Ling, F. and Zhang, T.: Impact of the timing and duration of seasonal snow cover on the active layer and permafrost in the Alaskan Arctic.  
627 *Permafrost Periglacial Process.*, 14(2), 141-150, 2003.
- 628 Macander, M.J., Swingley, C.S., Joly, K., and Reynolds, M.K.: Landsat-based snow persistence map for northwest Alaska. *Remote Sens.  
629 Environ.*, 163, 23-31, 2015.



- 630 Mackay, J.R.: Catastrophic lake drainage, Tuktoyaktuk Peninsula area, District of Mackenzie, Current Research, Part D. Geological Survey  
631 of Canada, 83-90, 1988.
- 632 Marsh, P., Russell, M., Pohl, S., Haywood, H., Onclin, C.: Changes in thaw lake drainage in the Western Canadian Arctic from 1950 to  
633 2000. *Hydrol. Process.* 23, 145-158, 2009.
- 634 Melvin, A.M., Larsen, P., Boehlert, B., Neumann, J.E., Chinowsky, P., Espinet, X., Martinich, J., Baumann, M.S., Rennels, L., Bothner, A.,  
635 and Nicolsky, D.J.: Climate change damages to Alaska public infrastructure and the economics of proactive adaptation. *Proceedings of the*  
636 *National Academy of Sciences*, 114(2), E122-E131, 2017.
- 637 Ménard, P., Duguay, C.R., Flato, G.M., and Rouse, W.R.: Simulation of ice phenology on Great Slave Lake, Northwest Territories, Canada.  
638 *Hydrol. Process.*, 16(18), 3691-3706, 2002.
- 639 Menne, M.J., I. Durre, B. Korzeniewski, S. McNeal, K. Thomas, X. Yin, S. Anthony, R. Ray, R.S. Vose, B.E. Gleason, and T.G. Houston:  
640 Global Historical Climatology Network - Daily (GHCN-Daily), Version 3. NOAA National Climatic Data Center.  
641 <http://doi.org/10.7289/V5D21VHZ> [2019-09-03], 2012.
- 642 Nitze, I. and Grosse, G.: Detection of landscape dynamics in the Arctic Lena Delta with temporally dense Landsat time-series stacks. *Remote*  
643 *Sens. Environ.*, 181, 27-41, 2016.
- 644 Nitze, I., Grosse, G., Jones, B.M., Arp, C., Ulrich, M., Fedorov, A., and Veremeeva, A.: Landsat-based trend analysis of lake dynamics  
645 across northern permafrost regions. *Remote Sens.*, 9(7), p.640, 2017.
- 646 Nitze, I., Grosse, G., Jones, B.M., Romanovsky, V.E., and Boike, J.: Remote sensing quantifies widespread abundance of permafrost region  
647 disturbances across the Arctic and Subarctic. *Nat. Commun.*, 9(1), p.5423, 2018a.
- 648 Nitze, I., Grosse, G., Jones, B.M., Romanovsky, V.E., and Boike, J.: Remote sensing quantifies widespread abundance of permafrost region  
649 disturbances across the Arctic and Subarctic, *Datasets*, PANGAEA, <https://doi.org/10.1594/PANGAEA.894755>, 2018b.
- 650 Obu, J., Westermann, S., Bartsch, A., Berdnikov, N., Christiansen, H.H., Dashtseren, A., Delaloye, R., Elberling, B., Eitzelmüller, B.,  
651 Kholodov, A., and Khomutov, A.: Northern Hemisphere permafrost map based on TTOP modelling for 2000–2016 at 1 km<sup>2</sup> scale. *Earth-*  
652 *Science Reviews*, 2019.
- 653 Olthof, I., Fraser, R.H., and Schmitt, C.: Landsat-based mapping of thermokarst lake dynamics on the Tuktoyaktuk Coastal Plain, Northwest  
654 Territories, Canada since 1985. *Remote Sens. Environ.*, 168, 194-204, 2015.
- 655 Osterkamp, T.E.: Characteristics of the recent warming of permafrost in Alaska, *J. Geophys. Res.*, 112, F02S02, doi:10.1029/2006JF000578,  
656 2007.
- 657 Parsekian, A.D., Jones, B.M., Jones, M., Grosse, G., Walter Anthony, K.M., and Slater, L.: Expansion rate and geometry of floating  
658 vegetation mats on the margins of thermokarst lakes, northern Seward Peninsula, Alaska, USA. *Earth Surface Processes and Landforms*, 36,  
659 1889-1897, 2011.
- 660 Pastick, N.J., Jorgenson, M.T., Goetz, S.J., Jones, B.M., Wylie, B.K., Minsley, B.J., Genet, H., Knight, J.F., Swanson, D.K., and Jorgenson,  
661 J.C.: Spatiotemporal remote sensing of ecosystem change and causation across Alaska. *Glob. Chang. Biol.*, 25(3), 1171-1189, 2019.
- 662 Planet Team: Planet Application Program Interface: In Space for Life on Earth. San Francisco, CA. <https://api.planet.com>, 2017.
- 663 Plug, L.J., Walls, C., and Scott, B.M.: Tundra lake changes from 1978 to 2001 on the Tuktoyaktuk Peninsula, western Canadian Arctic.  
664 *Geophys. Res. Lett.*, 35, L03502, 2008.
- 665 Plug, L.J. and J. J. West: Thaw lake expansion in a two-dimensional coupled model of heat transfer, thaw subsidence, and mass movement,  
666 *J. Geophys. Res.*, 114, F01002, 2009.
- 667 QGIS Development Team. QGIS Geographic Information System. Open Source Geospatial Foundation Project. <https://qgis.osgeo.org>, 2019.



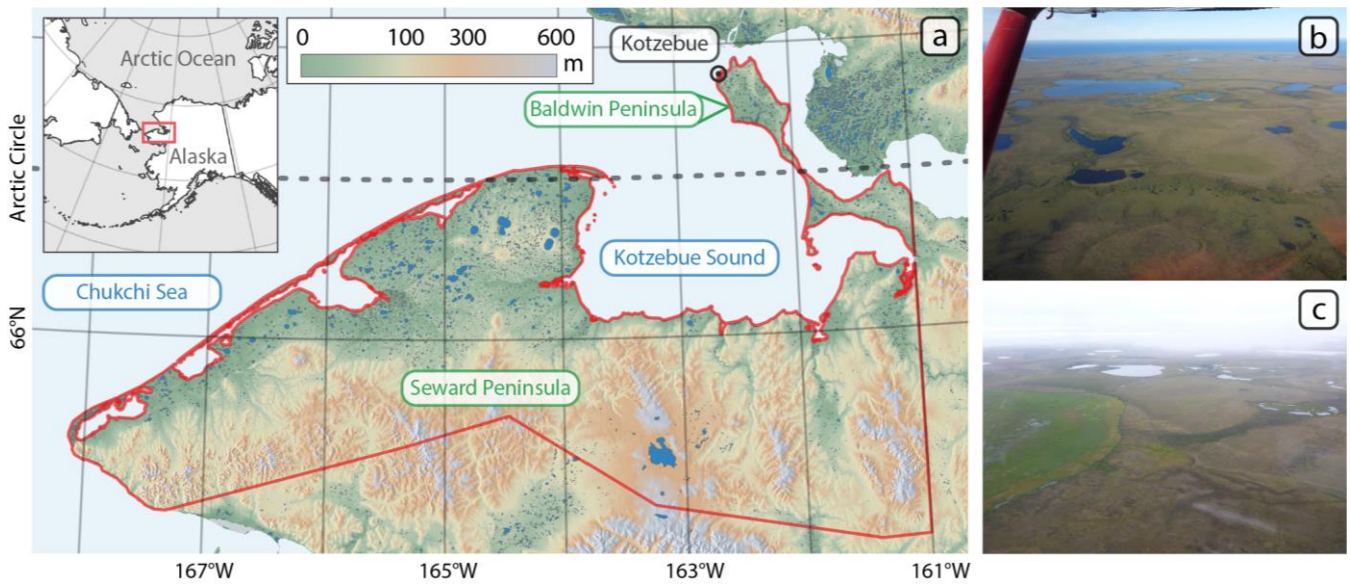
- 668 Regmi P., Grosse G., Jones M.C., Jones B.M., Walter Anthony K.M.: Characterizing Post-Drainage Succession in Thermokarst Lake Basins  
669 on the Seward Peninsula, Alaska with TerraSAR-X Backscatter and Landsat-based NDVI Data. *Remote Sens.*, 4(12): 3741-3765. doi:  
670 10.3390/rs4123741, 2012.
- 671 Repo, M.E., Susiluoto, S., Lind, S.E., Jokinen, S., Elsakov, V., Biasi, C., Virtanen, T., and Martikainen, P.J.: Large N<sub>2</sub>O emissions from  
672 cryoturbated peat soil in tundra. *Nature Geosci.*, 2, 189-192, 2009.
- 673 Roach, J.K., Griffith, B., and Verbyla, D.: Landscape influences on climate-related lake shrinkage at high latitudes. *Glob. Chang. Biol.*,  
674 19(7), 2276-2284, 2013.
- 675 Romanovsky, V.E., Smith, S.L., and Christiansen, H.H.: Permafrost thermal state in the polar Northern Hemisphere during the international  
676 polar year 2007-2009: a synthesis. *Permafrost Periglacial Process.*, 21, 106-116, 2010.
- 677 Shur, Y.L. and Jorgenson, M.T.: Patterns of permafrost formation and degradation in relation to climate and ecosystems. *Permafrost*  
678 *Periglacial Process.*, 18, 7-19, 2007.
- 679 Schuur, E.A., McGuire, A.D., Schädel, C., Grosse, G., Harden, J.W., Hayes, D.J., Hugelius, G., Koven, C.D., Kuhry, P., Lawrence, D.M.,  
680 and Natali, S.M.: Climate change and the permafrost carbon feedback. *Nature*, 520(7546), 171-179, 2015.
- 681 Scenarios Network for Alaska and Arctic Planning, University of Alaska. Retrieved 1 October 2019 from  
682 [http://ckan.snap.uaf.edu/dataset?q=decadal+2km&tags=annual&tags=AR5%2FCMIP5&tags=climate&sort=score+desc%2C+metadata\\_m](http://ckan.snap.uaf.edu/dataset?q=decadal+2km&tags=annual&tags=AR5%2FCMIP5&tags=climate&sort=score+desc%2C+metadata_modified+desc)  
683 [odified+desc](http://ckan.snap.uaf.edu/dataset?q=decadal+2km&tags=annual&tags=AR5%2FCMIP5&tags=climate&sort=score+desc%2C+metadata_modified+desc), 2020.
- 684 Smith, L.C., Sheng, Y., MacDonald, G.M., and Hinzman, L.D.: Disappearing arctic lakes. *Science*, 308(5727), 1429-1429, 2005.
- 685 Stabenow, P. J. and Bell, S. W.: Extreme Conditions in the Bering Sea (2017–2018): Record-Breaking Low Sea-Ice Extent. *Geophys. Res.*  
686 *Let.*, 2019.
- 687 Stieglitz, M., Déry, S.J., Romanovsky, V.E., and Osterkamp, T.E.: The role of snow cover in the warming of arctic permafrost. *Geophys.*  
688 *Res. Lett.*, 30(13), 2003.
- 689 Streletskiy, D.A., Shiklomanov, N.I., Little, J.D., Nelson, F.E., Brown, J., Nyland, K.E., and Klene, A.E.: Thaw Subsidence in Undisturbed  
690 Tundra Landscapes, Barrow, Alaska, 1962-2015. *Permafrost Periglacial Process.*, 28, 566-572, 2017.
- 691 Sturm, M. and Liston, G. E.: The snow cover on lakes of the Arctic Coastal Plain of Alaska, USA. *J. Glaciol.*, 49(166), 370-380, 2003.
- 692 Surdu, C.M., Duguay, C.R., Brown, L.C., and Prieto, D.F.: Response of ice cover on shallow lakes of the North Slope of Alaska to  
693 contemporary climate conditions (1950-2011): Radar remote-sensing and numerical modeling data analysis. *The Cryosphere*, 8(1), 167,  
694 2014.
- 695 Swanson, D.K.: Thermokarst and precipitation drive changes in the area of lakes and ponds in the National Parks of northwestern Alaska,  
696 1984–2018. *Arct., Antarc., Alp. Res.*, 51(1), 265-279, 2019.
- 697 Tape, K.D., Jones, B.M., Arp, C.D., Nitze, I., and Grosse, G.: Tundra be dammed: Beaver colonization of the Arctic. *Glob. Chang. Biol.*,  
698 24(10), 4478-4488, 2018.
- 699 Walker, D. A., Reynolds, M. K., Daniëls, F. J., Einarsson, E., Elvebakk, A., Gould, W. A., ..., and Moskalenko, N. G.: The circumpolar  
700 Arctic vegetation map. *Journal of Vegetation Science*, 16(3), 267-282, 2005.
- 701 Walter Anthony, K., von Deimling, T.S., Nitze, I., Frolking, S., Emond, A., Daanen, R., Anthony, P., Lindgren, P., Jones, B., and Grosse,  
702 G.: 21st-century modeled permafrost carbon emissions accelerated by abrupt thaw beneath lakes. *Nat. Commun.*, 9(1), p.3262, 2018.
- 703 Wetterich S., Grosse G., Schirmermeister L., Andreev A.A., Bobrov A.A., Kienast F., Bigelow N.H., and Edwards M.E.: Late Quaternary  
704 environmental and landscape dynamics revealed from a pingo sequence on the Seward Peninsula, Alaska. *Quat. Sci. Rev.*, 39: 26-44. doi:  
705 10.1016/j.quascirev.2012.01.027, 2012.



- 706 White, D.M., Gerlach, S.C., Loring, P., Tidwell, A.C., and Chambers, M.C.: Food and water security in a changing arctic climate. Environ.  
707 Res. Lett., 2, 045018, 2007.
- 708 Yoshikawa, K. and Hinzman, L.D.: Shrinking thermokarst ponds and groundwater dynamics in discontinuous permafrost near Council,  
709 Alaska. Permafrost Periglacial Process., 14(2), 151-160, 2003.
- 710



711



712

713

714

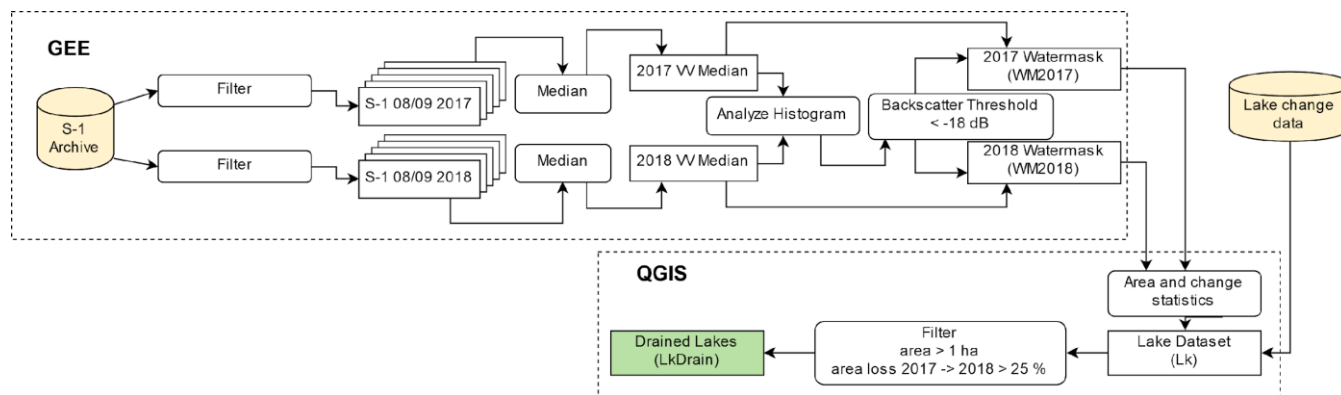
715

**Figure 1: a) Overview of study area with topography and place names. Elevation source: GMTED2010. b) Oblique aerial photo of the formerly largest lake on the Baldwin Peninsula, which drained in 2018. Photo: J.Strauss, July 2016. c) Oblique aerial photo of the northern Seward Peninsula. Photo: G.Grosse, July 2016. Lake-rich permafrost landscape with large drained basin.**

716



717



718

719

720

721

**Figure 2: Flowchart of lake change detection and drainage assignment based on Sentinel-1 data (S-1 Archive). Raster data processing was carried out in Google Earthengine (GEE). Lake vector extraction and calculation of recent and historic (Lake change data: Nitze et al., 2018b) lake change statistics was carried out in Quantum GIS (QGIS).**

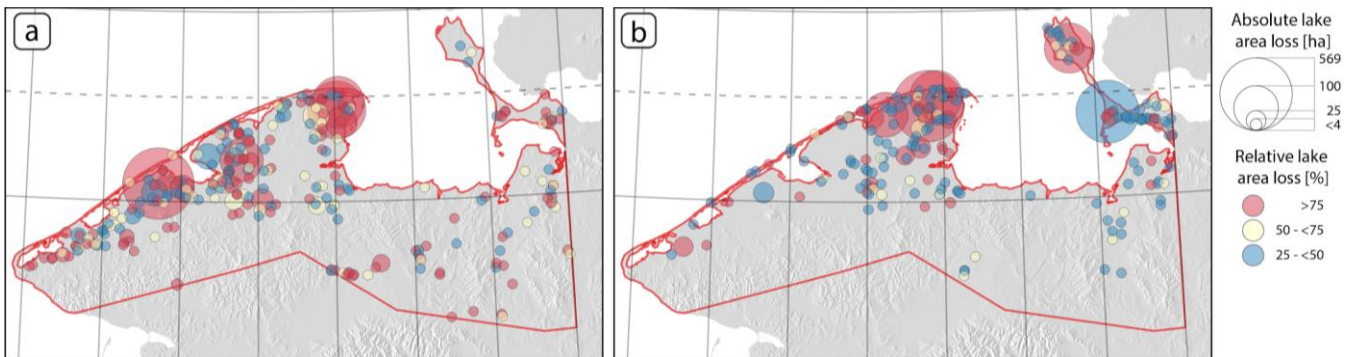
722

723

724



725



726

727

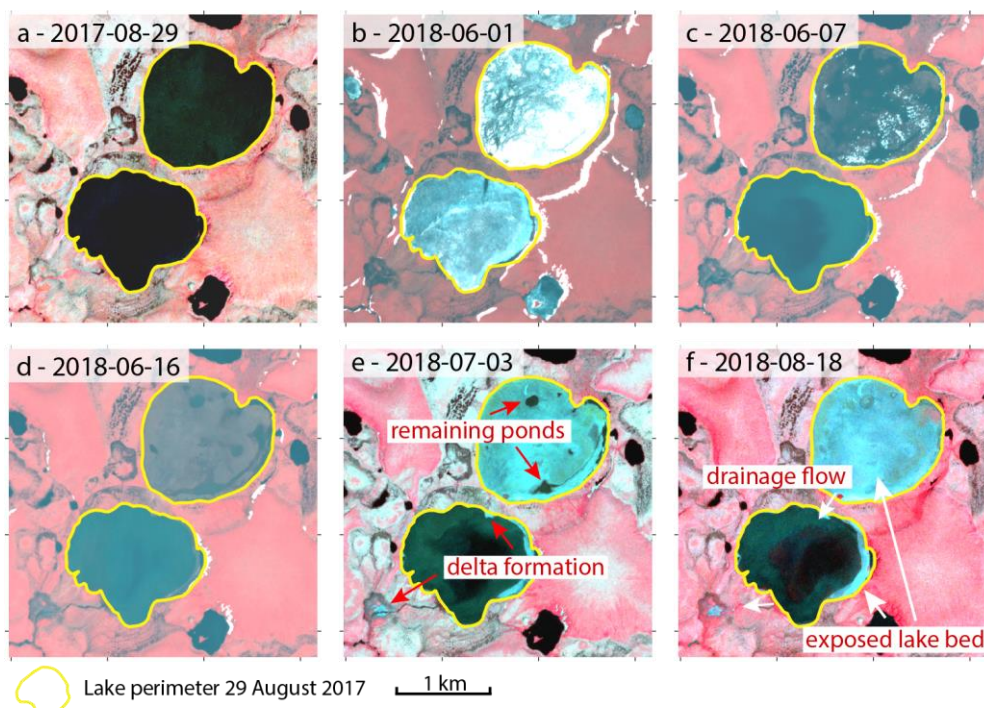
728

**Figure 3: Spatial patterns, size and percentage of drained lakes. a) 1999-2014, b) 2017-2018. Hillshade based on the GMTED2010 elevation dataset.**

729

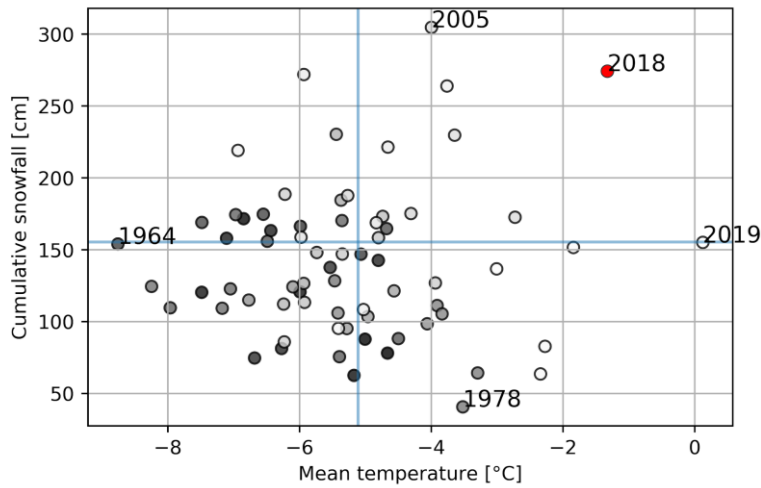


730



731

732 **Figure 4:** PlanetScope (Planet Team, 2017) satellite time-series of cascaded lake drainage of lakes 99492 (north) and 99522 (south)  
733 (66.45°N, 164.75°W) from 29 August 2017 until 18 August 2018 with annotations of drainage related features. a) Lakes before  
734 drainage. b) Ice-break-up with initial drainage pattern visible on the northern lake. c) Post ice-breakup with reduced water level in  
735 the northern lake. d) Northern lake nearly completely drained with few remaining ponds. e) Partial drainage of the southern lake  
736 with visible delta formation. f) Final stage of lake drainage with dried out ponds (northern lake) and lake level stabilization (southern  
737 lake).



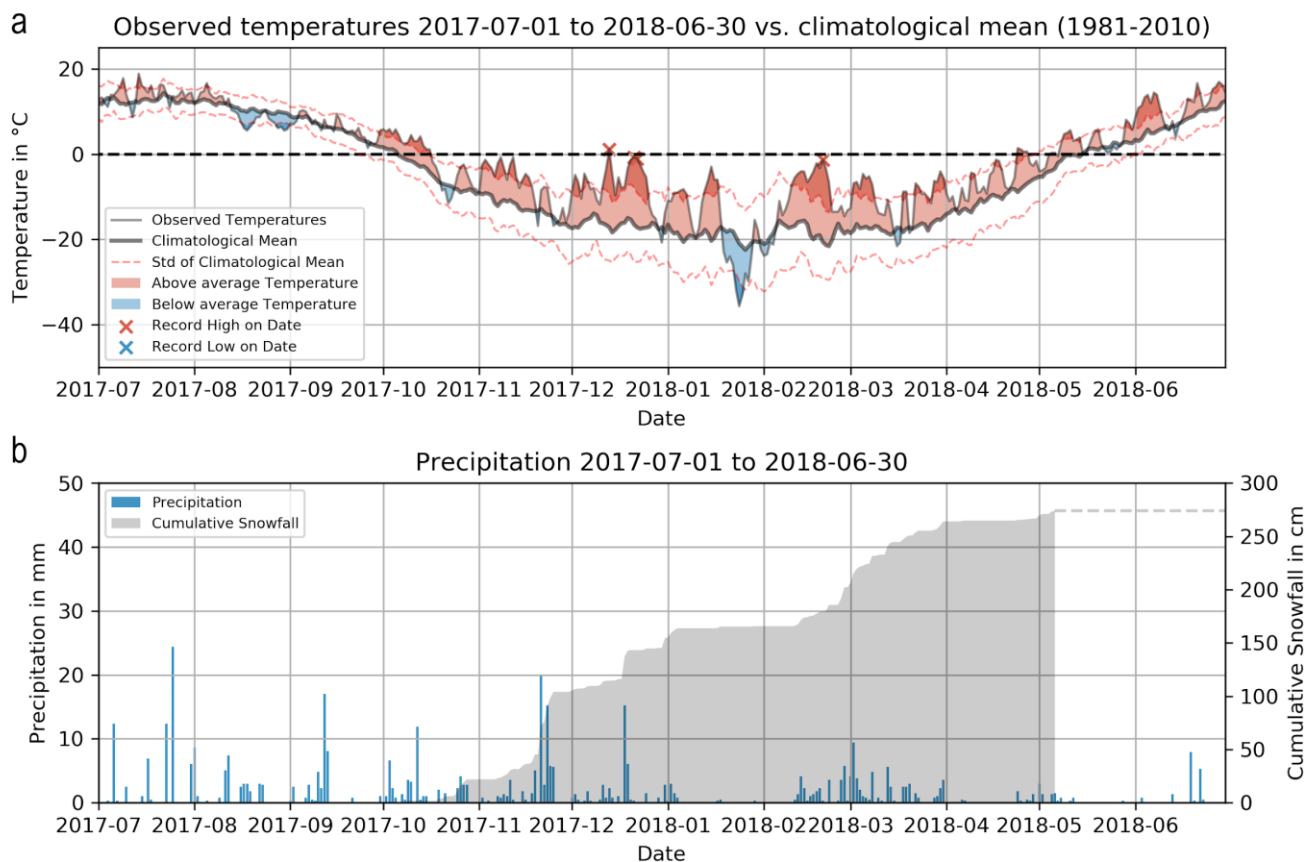
738  
739  
740  
741

**Figure 5: Scatterplot of mean air temperature and cumulative snowfall per winter year (July to June). Winter year 2017/2018 marked in red. Extreme years indicated by number. Blue lines indicate climatic means of MAAT and cumulative snowfall (1981-2010). Dots in greyscale indicate the year from 1934 (black) until 2019 (white).**



742

743



744

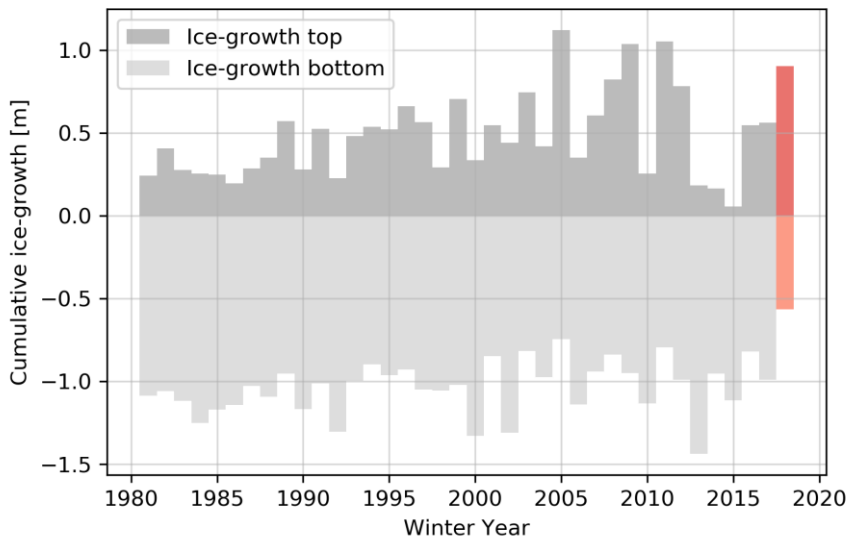
745

746

747

748

**Figure 6: Overview of winter weather conditions at Kotzebue climate station from July 1 2017 through June 30 2018. a) Observed temperatures in °C with anomaly (red: warmer, blue: colder) from climatological mean (1981-2010). Dark color shades indicate deviation of >1 standard deviation from the mean. Record temperatures for particular days are marked with an “x” b) Daily precipitation and cumulative snowfall.**



749

750

751

**Figure 7: Simulated cumulative top and bottom ice-growth per winter year for 100 % snow scenario in cm. Winter year 2017/2018 highlighted in red.**

752



753

754 **Table 1: Overview of datasets and for lake change analysis.**

Dataset	Abbreviation	Period	Source
Lake Change Dataset	Lk	1999-2014	Nitze et al. 2018b
Watermask Sentinel 1 2017	WM 2017	2017	
Watermask Sentinel 1 2018	WM 2018	2018	
Planet dynamic water mask	LkDyn	2017-2018	
Derived Lake change 2017-2018	LkDrain	1999-2018	

755

756 **Table 2: Lakes ranked by largest area loss from 2017 to 2018 with lake area rank 2017, Lake ID, net change area and percentage as**  
 757 **well as lake area in 2017 and 2018. For full dataset see Supplementary Table 1 and datasets LkDrain. \*Lagoon connected to the**  
 758 **sea/Kotzebue Sound.**

Drain rank	Lake area rank 2017	Lake ID	Net change 2017-2018 [ha]	Net change 2017-2018 [%]	Area 2017 [ha]	Area 2018 [ha]	Video animation
1	12	99368	-332.04	-91.24	363.92	31.88	<a href="#">Link</a>
2*	6	69152	-258.8	-34.31	754.36	495.56	<a href="#">Link</a>
3	32	99230	-185.12	-99.70	185.68	0.56	<a href="#">Link</a>
4	39	64656	-164.6	-99.83	164.88	0.28	<a href="#">Link</a>
5	51	99492	-132.12	-100	132.12	0	<a href="#">Link</a>
6	205	100218	-28.48	-78.24	36.4	7.92	<a href="#">Link</a>
7	105	101659	-27.56	-41.53	66.36	38.8	<a href="#">Link</a>
8	269	99545	-26.12	-97.32	26.84	0.72	<a href="#">Link</a>
9	281	102499	-25.72	-100	25.72	0	<a href="#">Link</a>
10	305	100470	-23.2	-100	23.2	0	<a href="#">Link</a>

759

760



761

762 **Table 3: Lakes with largest area loss from 1999 to 2014 with net change area and percentage as well as lake area of 1999 and 2014**  
763 **(Nitze et al., 2018b). For full datasets see Supplementary Table 2 and datasets Lk.**

<b>Drain Rank</b>	<b>Lake ID</b>	<b>Net change 1999-2014 [ha]</b>	<b>Net change 1999-2014 [%]</b>	<b>Area 1999 [ha]</b>	<b>Area 2014 [ha]</b>	<b>Year Drained</b>
1	101282	-568.92	-97.95	580.8	11.88	2007
2	99433	-373.29	-99.63	374.67	1.37	2006
3	99313	-299.98	-78.77	380.84	80.85	2006
4	100588	-208.53	-94.69	220.22	11.69	2004
5	99624	-113.43	-99.55	113.94	0.52	2006
6	101659	-79.32	-31.55	251.42	172.1	2009
7	99505	-76.16	-62.7	121.48	45.31	2003
8	100505	-74.27	-28.86	257.36	183.08	2003
9	101402	-65.62	-98.3	66.75	1.14	2003
10	101844	-56.5	-99.06	57.03	0.54	2004

764

765



766

767 **Table 4. Annually aggregated observations of mean air temperature, cumulative precipitation, cumulative snowfall, cumulative**  
 768 **freezing degree days, and freezing days per winter year (July 1 until June 30) for climate station Kotzebue, sorted by mean air**  
 769 **temperature. 10 warmest and 5 coldest years included. For full data (1950-2019) see Supplementary Table 3.**

Winter Year	Rank Temperature	Mean Air Temperature [°C]	Cumulative Precipitation [mm]	Cumulative Snowfall [cm]	Cumulative FDD	Freezing Days
2019	1	+0.12	278.6	155.1	-1755.50	181
2018	2	-1.33	424.5	274.2	-1904.75	196
2016	3	-1.84	258.1	151.6	-2142.85	200
2014	4	-2.27	260.5	82.8	-2136.75	178
2015	5	-2.34	247.8	63.6	-2428.80	208
2003	6	-2.73	244.0	172.6	-2262.85	195
2017	7	-3.01	225.0	136.7	-2631.05	194
1979	8	-3.29	207.5	64.3	-2648.80	221
1978	9	-3.52	210.9	40.7	-2795.10	206
2004	10	-3.64	313.5	229.7	-2698.15	181
1966	64	-7.48	262.7	169.0	-3642.30	240
1955	65	-7.48	305.9	120.4	-3711.65	225
1971	66	-7.96	160.3	109.6	-3975.45	237
1976	67	-8.25	199.7	124.5	-3923.10	239
1964	68	-8.76	300.6	154.0	-4130.00	227

770

771